Original Article

Integrated control of path tracking and handling stability for autonomous ground vehicles with four-wheel steering

Wenbo Li[1,2], Shuyou Yu[1,2] (iD), Lei Tan[2], Yongfu Li[3], Hong Chen[2,4] and Jianhua Yu[5]

Abstract

Accurate modelling of an autonomous ground vehicle (AGV) is challenging due to strong nonlinearity, model perturbations and external disturbances. This necessitates the design of path tracking controllers with robustness. In this paper, an integrated control strategy for path tracking and handling stability of AGVs is proposed, leveraging a four-wheel steering (4WS) system. To address the path tracking problem, a fuzzy logic-based steering strategy is developed, which enables parameter self-adjustment based on displacement error. Additionally, a reference model is employed to transform the path tracking problem into a reference signal tracking problem, ensuring the handling stability of vehicles. A sliding mode controller is designed to track the reference signal, utilizing an extended state observer to estimate and compensate for unmodeled dynamics and unknown external disturbances in real-time. Simulation results demonstrate the effectiveness of the proposed strategy in accurately tracking the desired path while maintaining the lateral stability of the vehicle. Furthermore, the strategy exhibits strong robustness against uncertainties and disturbances.

Introduction

Among the applications of intelligent transportation systems, the AGV has great advantages in terms of driving behaviour prediction, energy consumption and traffic accident reduction.[1] The technologies of the AGV include environment perception, path planning and path tracking.[2–4] One focus of the study is to design robust control strategies to track a reference path addressing the challenges posed by nonlinearity, uncertainty and disturbances in AGVs.[5]

Currently, much research has been proposed for path tracking of achieving strong robustness, including PID control, linear control method (such as preview-follower theory, triple-step control and H_∞ control) and nonlinear control method (such as sliding mode control and model predictive control). A robust controller utilizing a fractional-order proportional integral derivative method is explored,[6] where a kinematic model is adopted. The preview-follower theory based on a point-mass model has been adopted, which directly uses road information rather than vehicle dynamic information.[7–10] A triple-step controller, which handles model uncertainties and disturbances, is proposed.[11] Robust H_∞ controllers are presented,[12,13] which can deal with the parametric uncertainties in vehicles. The sliding mode control methods based on nonsingular terminal are investigated to achieve fast path tracking.[14–16]

[1]State Key Laboratory of Automotive Simulation and Control, Jilin University, Changchun, China
[2]Department of Control Science and Engineering, Jilin University, Changchun, China
[3]College of Automation, Chongqing University of Posts and Telecommunications, Chongqing, China
[4]College of Electronics & Information Engineering, Tongji University, Shanghai, China
[5]Dongfeng Commercial Vehicle Technology Center, Wuhan, China

Corresponding author:
Shuyou Yu, Department of Control Science and Engineering, Jilin University, No. 5988, Renmin Street, Changchun 130012, China.
Email: shuyou@jlu.edu.cn

A robust control method using nonsingular terminal-based sliding mode is discussed, which takes into account the uncertainties in vehicles.[17] Model predictive control, which has the advantage of explicitly handling kinematic constraints, dynamic constraints and actuator constraints of vehicles, is adopted to achieve path tracking.[18–20] Aiming at the path tracking problems of wheeled mobile robots, a receding horizon controller is designed,[21] in which both asymptotic convergence and feasibility of the optimization problem are proved. Deep learning methods have been applied in the path tracking for AGVs.[22,23] However, challenges such as the opaque nature, computational complexity and network architecture still need to be addressed.

Furthermore, enhancing vehicle handling stability is an effective approach to ensure safe operation of vehicles. Therefore, another focus of the study is to guarantee the handling stability of AGVs during the path tracking process. The chassis technologies can typically be categorized into three main methods: steering methods, suspension control methods and drive/brake control methods. Aiming at four-wheel-independent-drive electric vehicles, a composite control strategy is proposed, in which a nonlinear disturbance observer is designed to estimate the disturbance, and a super-twisting second-order sliding mode is designed for the path-tracking problem.[24] In particular, the 4WS technology has garnered significant attention due to its flexible steering mode, as it can effectively enhance vehicle handling stability and active safety. Currently, the handling stability control methods of 4WS vehicles can typically be categorized into feedforward control, that is, proportional control,[25] and feedforward and feedback control characterized by transforming the path tracking problem into a reference signal tracking problem.[26–29] Most studies adopt the direct provision of front wheel steering angle and only consider the control of the handling stability of vehicles with four-wheel steering system. However, those approaches fail to address the issue of autonomous vehicles being able to achieve accurate path tracking. Exceptionally, a control strategy is proposed for 4WS vehicles, utilizing a PID driver model to follow the reference path accurately.[29] In addition, a triple-step controller is designed to effectively track the reference signals. Nevertheless, this approach ignores unmeasured states, uncertainties and disturbances in vehicles.

Although extensive research has been conducted in the field of AGVs, there are still several critical issues that require consideration. Accurately modelling AGVs with 4WS is a challenging task due to strong nonlinearity, model perturbations and external disturbances. Therefore, the design of a robust control strategy is crucial to achieve precise path tracking while ensuring the handling stability of 4WS vehicles. This paper introduces an integrated control strategy for AGVs that takes into account both path tracking performance and handling stability. For clarity and convenience in subsequent discussions, we will use the abbreviation 'LSC' (lateral stability controller) to refer to this strategy. The main contributions of this paper are as follows:

(1) The proposed controller enables dynamic adjustment of the parameters of the steering controller based on the AGV's path tracking performance.
(2) To enhance the active safety and handling stability of AGVs, an extended state observer-based sliding mode control (ESO-SMC) is proposed. The uncertainties in the AGV are modelled as lumped disturbance terms and estimated using an extended state observer (ESO). Additionally, the convergence stability of the ESO-SMC is rigorously proven.

The rest of this paper is structured as follows: Section 'Problem setup' is the problem setup. Section 'Lateral stability controller' introduces the design process of the lateral stability controller. Section 'Simulation' verifies the effectiveness of the proposed controller through simulation. The conclusion is drawn in Section 'Conclusion'.

Problem setup

The control objectives of AGVs include path tracking and lateral stability improvement As shown in Figure 1, the total framework of the proposed scheme includes four modules. (1) According to the reference path f_{road}, vehicle's lateral displacement Y and lateral velocity $\dot{Y}$, the steering strategy first determines the reference front wheel angle δ_f^*. (2) The reference model constructs the reference signals according to the reference front wheel angle, that is, β^* and γ^*, and transforms the path tracking problem into the tracking problem of reference signals. (3) The extended state observer simultaneously observes lumped disturbances and unmeasured states. (4) An ESO-SMC is designed to accurately track the reference signal in the presence of disturbances. The proposed scheme can track the reference path.

Remark 1. *The steering strategy module gives a reference front wheel angle that can make the vehicle track the reference path, which directly determines the performance of path tracking. Additionally, the reference model provides reference signals for a front-wheel angle. It ensures that the driving trajectory of the 4WS vehicle remains consistent with that of the front-wheel steering vehicle and maintains vehicle handling stability. The ESO-SMC is designed to robustly track the above reference signals, which indirectly affects the vehicle trajectory.*

Remark 2. *Note that the reference path is determined by path planning based on environmental perception, which is out of the scope of this paper.*

Lateral stability controller

Steering strategy based on Fuzzy logics

The steering strategy is designed based on the single-point preview model. Considering the model
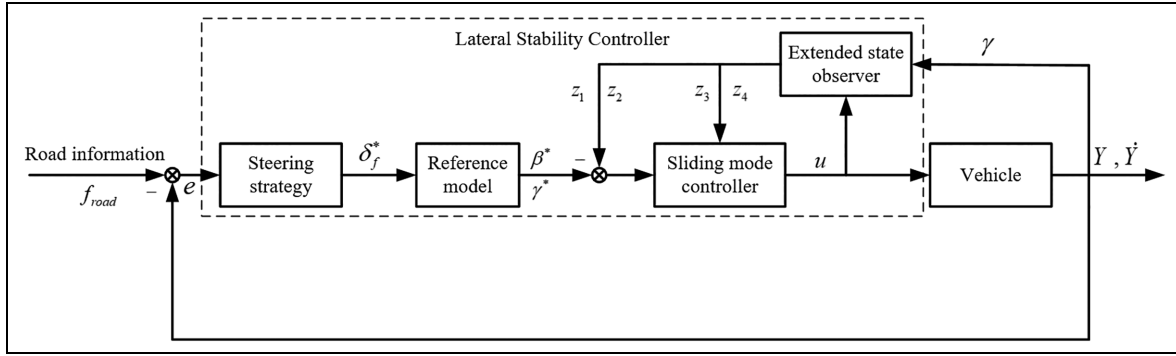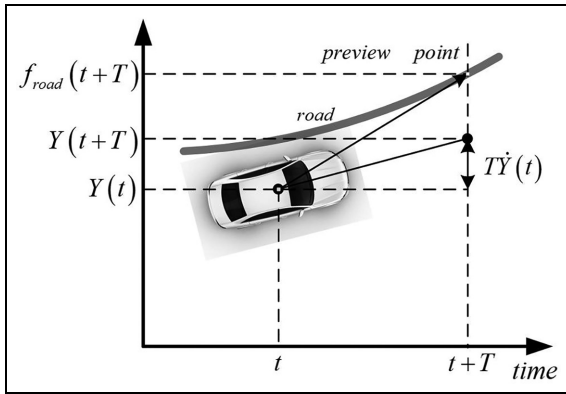
Figure 1. The control system of AGVs.

Figure 2. Deviation diagram of driving trajectory.

Figure 3. Steering strategy.

Figure 4. Membership function of $e, \dot{e}, \Delta k_p, \Delta k_i, \Delta k_d$.

complexity, time delay and nonlinearity of vehicles, the steering strategy combined with fuzzy algorithm and PID control is proposed, which can achieve self-tuning of parameters.

The deviation diagram of vehicle driving trajectory is shown in Figure 2, where $Y(t)$ is the vehicle's lateral displacement, $\dot{Y}(t)$ is the vehicle's lateral velocity, t is the time instant, $f_{road}(t + T)$ represents the preview point and T is the preview time.

Define the road deviation as

$$e(t) = f_{road}(t + T) - Y(t + T) \tag{1}$$

Since $Y(t + T) - Y(t) \approx T\dot{Y}(t)$,

$$e(t) \approx f_{road}(t + T) - Y(t) - T\dot{Y}(t) \tag{2}$$

With PID, the ideal front wheel angle is

$$\delta_f^* = k_p e(t) + k_i \int_0^t e(t)dt + k_d \frac{de(t)}{dt} \tag{3}$$

where k_p is the proportional gain, k_i is the integral gain and k_d is the derivative gain.

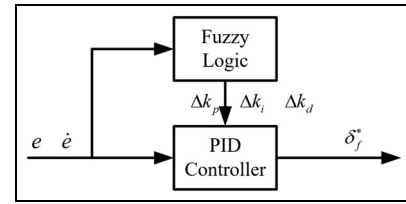Furthermore, a fuzzy logic is adopted to regulate the PID parameters online.[30,31] The framework of the steering strategy of the AGV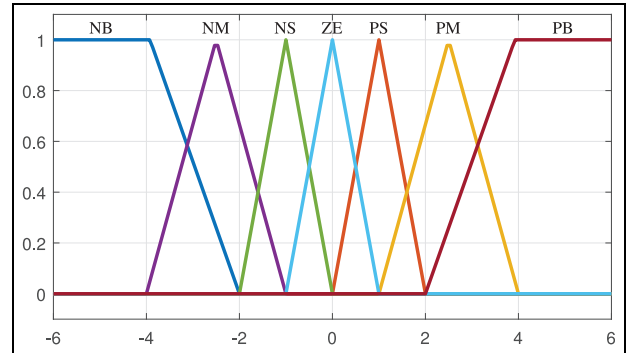 is shown in Figure 3, where the road deviation e and deviation derivative $\dot{e}$ are the input variables of fuzzy logic as well. The fuzzy logic modifies values of k_p, k_i, k_d, that is, incremental variables $\Delta k_p, \Delta k_i, \Delta k_d$ are set by fuzzy logic.

Define the domain scopes of $e, \dot{e}, \Delta k_p, \Delta k_i, \Delta k_d$ as $[-6, 6]$. The fuzzy variables can be expressed as

$$[NB \quad NM \quad NS \quad ZO \quad PS \quad PM \quad PB]$$

which present negative big, negative medium, negative small, zero, positive small, positive medium and positive big, respectively. The membership functions of all parameters are in triangular distribution, as shown in Figure 4.

Define the domain scopes of $e, \dot{e}, \Delta k_p, \Delta k_i, \Delta k_d$ as $[-6, 6]$. The fuzzy rules of $\Delta k_p, \Delta k_i, \Delta k_d$ are shown in Tables 1 to 3.

Table 1. Fuzzy control rule of Δk_p.

$\dot{e}$ Δk_p e	NB	NM	NS	ZO	PS	PM	PB
NB	PB	PB	PM	PM	PS	ZO	ZO
NM	PB	PB	PM	PS	PS	ZO	NS
NS	PB	PM	PM	PS	ZO	NS	NS
ZO	PM	PM	PS	ZO	NS	NM	NM
PS	PS	PS	ZO	NS	NS	NM	NB
PM	PS	ZO	NS	NM	NM	NM	NB
PB	ZO	ZO	NM	NM	NM	NB	NB

Table 2. Fuzzy control rule of Δk_i.

$\dot{e}$ Δk_i e	NB	NM	NS	ZO	PS	PM	PB
NB	NB	NB	NM	NM	NS	ZO	ZO
NM	NB	NB	NM	NS	NS	ZO	ZO
NS	NB	NM	NS	NS	ZO	PS	PS
ZO	NM	NM	NS	ZO	PS	PM	PM
PS	NS	NS	ZO	PS	PS	PM	PB
PM	ZO	ZO	PS	PS	PM	PB	PB
PB	ZO	ZO	PS	PM	PM	PB	PB

Table 3. Fuzzy control rule of Δk_d.

$\dot{e}$ Δk_d e	NB	NM	NS	ZO	PS	PM	PB
NB	PS	NS	NB	NB	NB	NM	PS
NM	PS	NS	NB	NM	NM	NS	ZO
NS	ZO	NS	NM	NM	NS	NS	ZO
ZO	ZO	NS	NS	NS	NS	NS	ZO
PS	ZO	ZO	ZO	ZO	ZO	ZO	ZO
PM	PB	NS	PS	PS	PS	PS	PB
PB	PB	PM	PM	PM	PS	PS	PB

Then, the ideal front wheel steering angle is

$$\delta_f^* = k_p^* e(t) + k_i^* \int_0^t e(t)dt + k_d^* \frac{de(t)}{dt} \tag{4}$$

where $k_p^* = k_p + \Delta k_p$, $k_i^* = k_i + \Delta k_i$ and $k_d^* = k_d + \Delta k_d$.

Reference model

The ideal steering characteristic of vehicles has the ideal steering sensitivity and stable vehicle body attitude. In this subsection, a reference model is established, which transforms the ideal front wheel angle to an ideal yaw rate and an ideal sideslip angle, that is, transforms the path tracking problem into a reference signal tracking problem.[32,33]

$$\dot{x}_d = A_d x_d + B_d u_d \tag{5}$$

with

$$A_d = \begin{bmatrix} -\frac{1}{\tau_\beta} & 0 \\ 0 & -\frac{1}{\tau_\gamma} \end{bmatrix}, B_d = \begin{bmatrix} \frac{k_\beta}{\tau_\beta} \\ \frac{k_\gamma}{\tau_\gamma} \end{bmatrix}$$

where $x_d = [\beta^* \quad \gamma^*]^T$ and $u_d = [\delta_f^*]$ respectively represent the state and input of reference model, γ^* is the ideal yaw rate, β^* is the ideal sideslip angle, δ_f^* is the ideal front wheel angle,

$$k_\gamma = \frac{k_f k_r (a + b)v}{k_f k_r (a + b)^2 - mv^2 (ak_f - bk_r)}$$

is the steady state gain, τ_β and τ_γ are the time constants, k_β is the ideal centroid sideslip angle gain.

ESO-SMC

Aiming at tracking the reference signals, that is, β^* and γ^*, and observing disturbances and unmeasured states in AGVs, an ESO-SMC is presented.

Vehicle model. Supposing that the longitudinal speed is constant. As shown in Figure 5, a two degree-of-freedom (DOF) vehicle model based on a four-wheel steering (4WS) chassis technology is presented.[34,35] Compared with the front-wheel steering vehicle, the 4WS can effectively improve the lateral stability and active safety of the vehicle.[26,36]

$$\begin{cases} mv_x(\dot{\beta} + \gamma) = -\left(k_f + k_r\right)\beta - \dfrac{\gamma}{v_x}\left(ak_f - bk_r\right) \\ \qquad\qquad + k_f\delta_f + k_r\delta_r + F_d \\ I_z\dot{\gamma} = -\left(ak_f - bk_r\right)\beta - \dfrac{\gamma}{v_x}\left(a^2k_f - b^2k_r\right) \\ \qquad\qquad + ak_f\delta_f - bk_r\delta_r + l_wF_d \end{cases} \tag{6}$$

where m is the vehicle mass, α_f and α_r are the sideslip angles of the front and rear tyre respectively, F_{yf} and F_{yr} are tyre lateral forces, a and b are the distance from the centre of gravity to the front and rear axle respectively, β is the sideslip angle in the vehicle body, v_x is longitudinal speed, v_y is the lateral speed, γ is the yaw rate, I_z is the yaw moment of inertia, l_w represents the horizontal distance from the centre of the wind pressure to the centre of mass of vehicle, F_d represents the transverse force caused by the crosswind and X is the longitudinal displacement.

Denote the state vector $x = \begin{bmatrix} \beta & \gamma \end{bmatrix}^T$, and choose the system output $y = \gamma$. The vehicle model (6) is rewritten as

$$\begin{aligned} \dot{x} &= Ax + Bu + E_1F_d \\ y &= Cx \end{aligned} \tag{7}$$

where

$$A = \begin{bmatrix} -\dfrac{k_f + k_r}{mv_x} & \dfrac{bk_r - ak_f}{mv_x^2} - 1 \\ \dfrac{bk_r - ak_f}{I_z} & -\dfrac{a^2k_f + b^2k_r}{I_zv_x} \end{bmatrix},$$

$$B = \begin{bmatrix} \dfrac{k_f}{mv_x} & \dfrac{k_r}{mv_x} \\ \dfrac{ak_f}{I_z} & -\dfrac{bk_r}{I_z} \end{bmatrix}, \tag{8}$$

$$E_1 = \begin{bmatrix} \dfrac{1}{mv_x} & \dfrac{l_w}{I_z} \end{bmatrix}^T, C = \begin{bmatrix} 0 & 1 \end{bmatrix},$$

and $u = \begin{bmatrix} \delta_f & \delta_r \end{bmatrix}^T$ is the system input.

Considering the modelling uncertainties, the vehicle model (7) can be reformulated as

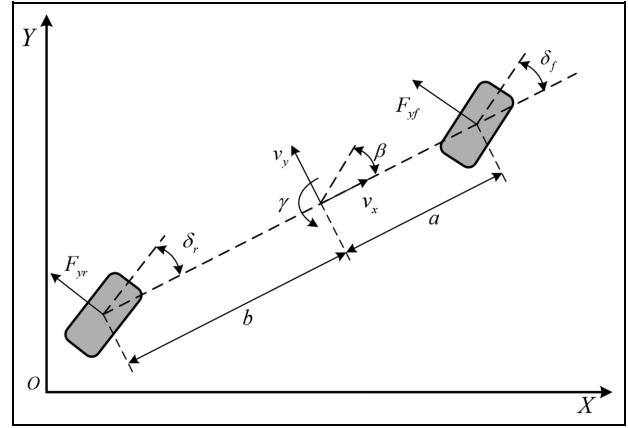$$\begin{aligned} \dot{x} &= [A + \Delta A]x + [B + \Delta B]u + E_1F_d \\ y &= Cx \end{aligned} \tag{9}$$

Figure 5. Two degree-of-freedom vehicle model.

where ΔA and ΔB represent the parametric perturbations.

Then, (9) can be reformulated as

$$\begin{aligned} \dot{x} &= Ax + B[u + d] \\ y &= Cx \end{aligned} \tag{10}$$

where $d = \begin{bmatrix} d_1 & d_2 \end{bmatrix}^T$ represents the lumped disturbance that contains external disturbances and modelling errors.[37]

Remark 3. *The system dynamics with parametric perturbations can be represented by the tracking state equation*

$$\dot{x} = [A + \Delta A]x + [B + \Delta B]u \tag{11}$$

where $x \in \Re^n$ is the state vector, $u \in \Re^r$ is the known input vector, $A \in \Re^{n \times n}$, $\Delta A \in \Re^{n \times n}$, $B \in \Re^{n \times r}$ and $\Delta B \in \Re^{n \times r}$.

The parametric perturbations can be represented as[38]

$$\begin{aligned} \Delta A(t) &= \sum_{i=1}^{N_A} a_i(t)A_i \\ \Delta B(t) &= \sum_{i=1}^{N_B} b_i(t)B_i \end{aligned} \tag{12}$$

where $\{A_1, \cdots, A_i\}$ is the basis of the real number field $R^{n \times n}$, $N_A = n \times n$, $\{B_1, \cdots, B_i\}$ is the basis of the real number field $R^{n \times r}$, $N_B = n \times r$, a_i and b_i are scalar time varying factors. Each equation of (12) is given by a linear combination of those scalar time varying factors with constant matrices A_i and B_i.

Thus, the parametric variations can be represented by the unknown input term, that is,

$$E_2d_p(t) = \Delta Ax + \Delta Bu$$

where

$$E_2 = \begin{bmatrix} A_1 & \cdots & A_{N_A} & B_1 & \cdots & B_{N_B} \end{bmatrix}$$

and

$$d_p(t) = \begin{bmatrix} a_1(t)x & \cdots & a_{N_A}(t)x & b_1(t)u & \cdots & b_{N_B}(t)u \end{bmatrix}^T$$

Then, the system dynamics with parametric perturbations can be rewritten as

$$\dot{x} = Ax + Bu + E_2 d_p$$

Thus, the lumped disturbance d in (10) is

$$d = \begin{bmatrix} d_1 & d_2 \end{bmatrix}^T = B^{-1} \begin{bmatrix} E_1 F_d + E_2 d_p \end{bmatrix}$$

The ESO is established as follows, which can simultaneously observe the unmeasurable state β and the disturbance d. The system (10) is rewritten as

$$\begin{aligned}
\dot{x}_1 &= a_{11}x_1 + a_{12}x_2 + b_{11}u_1 + b_{12}u_2 + b_{11}d_1 + b_{12}d_2 \\
\dot{x}_2 &= a_{21}x_1 + a_{22}x_2 + b_{21}u_1 + b_{22}u_2 + b_{21}d_1 + b_{22}d_2 \\
y &= x_2
\end{aligned} \tag{13}$$

where $x_1 = \beta$, $x_2 = \gamma$, $u_1 = \delta_f$, $u_2 = \delta_r$, a_{ij} and b_{ij} are the coefficients of the $i-$ th row and the $j-$ th column of the matrix A and B respectively, $i, j \in \{1, 2\}$.

Define the disturbances of d_1 and d_2 extra two extended states x_3 and x_4, respectively, that is, $x_3 = d_1$ and $x_4 = d_2$, and rewrite (13) as

$$\begin{aligned}
\dot{x}_1 &= a_{11}x_1 + a_{12}x_2 + b_{11}u_1 + b_{12}u_2 + b_{11}x_3 + b_{12}x_4 \\
\dot{x}_2 &= a_{21}x_1 + a_{22}x_2 + b_{21}u_1 + b_{22}u_2 + b_{21}x_3 + b_{22}x_4 \\
\dot{x}_3 &= \varphi_1 \\
\dot{x}_4 &= \varphi_2 \\
y &= x_2
\end{aligned} \tag{14}$$

where φ_1 and φ_2 are the differential of d_1 and d_2 respectively.

An ESO for the system (14) is

$$\begin{aligned}
\dot{z}_1 &= a_{11}z_1 + a_{12}z_2 + b_{11}u_1 + b_{12}u_2 \\
&\quad + b_{11}z_3 + b_{12}z_4 - \alpha_1(\hat{y} - y) \\
\dot{z}_2 &= a_{21}z_1 + a_{22}z_2 + b_{21}u_1 + b_{22}u_2 \\
&\quad + b_{21}z_3 + b_{22}z_4 - \alpha_2(\hat{y} - y) \\
\dot{z}_3 &= -\alpha_3(\hat{y} - y) \\
\dot{z}_4 &= -\alpha_4(\hat{y} - y) \\
\hat{y} &= z_2
\end{aligned} \tag{15}$$

where α_1, α_2, α_3 and α_4 represent the observer gains, $\hat{y}$ is the output, z_1, z_2, z_3 and z_4 represent the observed values of x_1, x_2, d_1 and d_2. Note that d_1 and d_2 in (13) is approximated by z_3 and z_4.

Define an error system as

$$\dot{\varepsilon} = L\varepsilon + B_{\varphi 1}\varphi_1 + B_{\varphi 2}\varphi_2 \tag{16}$$

where $\varepsilon_i = x_i - z_i$, $i \in \{1, 2, 3, 4\}$,

$$L = \begin{bmatrix} a_{11} & a_{12} - \alpha_1 & b_{11} & b_{12} \\ a_{21} & a_{22} - \alpha_2 & b_{21} & b_{22} \\ 0 & -\alpha_3 & 0 & 0 \\ 0 & -\alpha_4 & 0 & 0 \end{bmatrix},$$

$$B_{\varphi 1} = \begin{bmatrix} 0 \\ 0 \\ 1 \\ 0 \end{bmatrix}, B_{\varphi 2} = \begin{bmatrix} 0 \\ 0 \\ 0 \\ 1 \end{bmatrix} \tag{17}$$

Denote the characteristic polynomial of the error system as $\lambda_0(s)$, and choose

$$\lambda_0(s) = |sI - L| = (s + \omega_0)^4 \tag{18}$$

where $\omega_0 > 0$.

Define the state of the error system

$$e_s = x_d - x = \begin{bmatrix} \beta^* - \beta & \gamma^* - \gamma \end{bmatrix}^T \tag{19}$$

The dynamics of the error system can be written as

$$\begin{aligned}
\dot{e}_s &= A_d x_d + B_d u_d - Ax - B[u + d] \\
&= A_d e_s + (A_d - A)x + B_d u_d - Bu - Bd
\end{aligned} \tag{20}$$

Define a sliding surface as

$$s = e_s + \lambda \int_0^t e_s(\tau)d\tau \tag{21}$$

where $s = \begin{bmatrix} s_1 & s_2 \end{bmatrix}^T$, and λ is a positive coefficient,

$$\lambda = \begin{bmatrix} \lambda_1 & 0 \\ 0 & \lambda_2 \end{bmatrix}$$

The system dynamics is

$$\dot{s} = \lambda e_s + \dot{e}_s \tag{22}$$

Due to (5), (10) and (19), (22) can be rewritten as

$$\dot{s} = \lambda e_s + A_d e_s + (A_d - A)x + B_d u_d - Bu - Bd \tag{23}$$

Due to

$$\begin{aligned}
d_1 &= z_3 + \varepsilon_3 \\
d_2 &= z_4 + \varepsilon_4
\end{aligned} \tag{24}$$

Then,

$$\dot{s} = \lambda e_s + A_d e_s + (A_d - A)x + B_d u_d - Bu - B \begin{bmatrix} z_3 + \varepsilon_3 \\ z_4 + \varepsilon_4 \end{bmatrix} \tag{25}$$

Choose the sliding mode controller as

$$u = B^{-1}\left[(\lambda + A_d)e_s + (A_d - A)x + B_d u_d - B[z_3 \quad z_4]^T - (\rho s + \eta \text{sgn}(s))\right] \tag{26}$$

That is,

$$u = B^{-1}\left[(\lambda + A_d)\begin{bmatrix} \beta^* - z_1 \\ \gamma^* - x_2 \end{bmatrix} + (A_d - A)\begin{bmatrix} z_1 \\ x_2 \end{bmatrix} + B_d u_d - B[z_3 \quad z_4]^T - (\rho s + \eta \text{sgn}(s))\right] \tag{27}$$

where x_2 is a measured variable, that is, yaw rate γ, x_1 is replaced by z_1 since x_1 can not be measured directly. The terms of z_3 and z_4 are the states of the ESO, ρ and η are undetermined coefficient with

$$\rho = \begin{bmatrix} \rho_1 & 0 \\ 0 & \rho_2 \end{bmatrix}, \quad \eta = \begin{bmatrix} \eta_1 & 0 \\ 0 & \eta_2 \end{bmatrix}$$

Therefore, the dynamics of system (22) can be rewritten as

$$\dot{s} = -\rho s - \eta \text{sgn}(s) - B[\varepsilon_3 \quad \varepsilon_4]^T \tag{28}$$

Analysis of robustness. Define a Lyapunov function

$$V := \frac{1}{2}s^2 \tag{29}$$

Then,

$$\begin{aligned} \dot{V} &= s\dot{s} \\ &= s\left(-\rho s - \eta \text{sgn}(s) - B\begin{bmatrix} \varepsilon_3 \\ \varepsilon_4 \end{bmatrix}\right) \\ &= -\rho_1 s_1^2 - \rho_2 s_2^2 - \eta_1|s_1| \\ &\quad -\eta_2|s_2| - \left([s_1 \quad s_2]B[\varepsilon_3 \quad \varepsilon_4]^T\right) \end{aligned} \tag{30}$$

Due to

$$\begin{aligned} &-\left(\left([s_1 \quad s_2]B\begin{bmatrix} \varepsilon_3 \\ \varepsilon_4 \end{bmatrix}\right)\right) \\ &\leqslant \left|[s_1 \quad s_2]B\begin{bmatrix} \varepsilon_3 \\ \varepsilon_4 \end{bmatrix}\right| \\ &= |s_1|(|b_{11}\varepsilon_3| + |b_{12}\varepsilon_4|) + \\ &\quad |s_2|(|b_{21}\varepsilon_3| + |b_{22}\varepsilon_4|) \end{aligned} \tag{31}$$

Hence,

$$\begin{aligned} \dot{V} &\leqslant -\rho_1 s_1^2 - \rho_2 s_2^2 - \eta_1|s_1| - \eta_2|s_2| + \\ &\quad |s_1|(|b_{11}\varepsilon_3| + |b_{12}\varepsilon_4|) + |s_2|(|b_{21}\varepsilon_3| + |b_{22}\varepsilon_4|) \\ &= -\rho_1 s_1^2 - \rho_2 s_2^2 - \\ &\quad (\eta_1 - |b_{11}\varepsilon_3| - |b_{12}\varepsilon_4|)|s_1| - \\ &\quad (\eta_2 - |b_{21}\varepsilon_3| - |b_{22}\varepsilon_4|)|s_2| \end{aligned} \tag{32}$$

Table 4. Parameters of vehicle.

Parameter	Value
Vehicle quality (m)	$1231kg$
Distance from centroid to front axle (a)	$1.035m$
Distance from centroid to rear axle (b)	$1.655m$
Yaw moment of inertia (I_z)	$3048.1kg \cdot m^2$
Front wheel cornering stiffness (k_f)	$39515.0N \cdot rad^{-1}$
Rear wheel cornering stiffness (k_r)	$39515.0N \cdot rad^{-1}$
Road adhesion coefficient	$[0.5, 0.9]$

Then, $\dot{V} \leqslant 0$ if the tracking conditions are satisfied

$$\begin{cases} \rho_1 > 0 \\ \rho_2 > 0 \\ \eta_1 > |b_{11}\varepsilon_3| + |b_{12}\varepsilon_4| \\ \eta_2 > |b_{21}\varepsilon_3| + |b_{22}\varepsilon_4| \end{cases} \tag{33}$$

Remark 4. *A smooth function* $con(s_i)^{39,40}$ *is used to alleviate chattering phenomenon.*

$$con(s_i) = \frac{s_i}{|s_i| + \varsigma} \quad i \in \{1, 2\} \tag{34}$$

where $\varsigma > 0$.
Then, the control law is

$$u = B^{-1}\left[(\lambda + A_d)\begin{bmatrix} \beta^* - z_1 \\ \gamma^* - x_2 \end{bmatrix} + (A_d - A)\begin{bmatrix} z_1 \\ x_2 \end{bmatrix} + B_d u_d - B[z_3 \quad z_4]^T - (\rho s + \eta con(s))\right]$$

Remark 5. *Note that the input matrix of the vehicle model with four-wheel steering chassis technology is invertible, which provides a necessary condition for the controller design.*

Simulation

In this section, a nonlinear 8 DOF vehicle model, which adopts the Dugoff tyre model, is chosen as the simulation model.[41] The vehicle parameters and controller parameters are shown in Tables 4 and 5, respectively.

As shown in Figure 6, the parameters $\eta_1 = 0.9$ and $\eta_2 = 10$ are selected. If the observation errors $|\varepsilon_3|$ and $|\varepsilon_4|$ satisfy $|b_{21}\varepsilon_3| + |b_{22}\varepsilon_4| < 10$, the conditions in (33) hold, that is,

$$\eta_1 > |b_{11}\varepsilon_3| + |b_{12}\varepsilon_4|$$
$$\eta_2 > |b_{21}\varepsilon_3| + |b_{22}\varepsilon_4|$$

Note that $\varepsilon_3 = x_3 - z_3$ and $\varepsilon_4 = x_4 - z_4$ shown in (16) are deviations of lumped disturbances and observed disturbances, which are small enough if the initial value of disturbance observer is chosen appropriately.

Table 5. Parameters of controller.

Parameter	Value	Parameter	Value
λ_1	800	λ_2	1000
ρ_1	600	ρ_2	500
η_1	0.9	η_2	10
k_p	0.23	k_i	0.002
k_d	0.035	ω_0	2100

Remark 6. *It should be noted that AGVs encompass a wide range of ground vehicles, including autonomous passenger vehicles, autonomous logistics vehicles and autonomous agricultural vehicles. The specifications of the 8 DOF vehicle model in this research are similar to those of a D-class passenger car.*

Case 1: Double lane change manoeuvre

In this subsection, a lane change manoeuvre is carried out for AGVs, which evaluates the path tracking and the lateral stability performance.

Scenario: the longitudinal speed of the vehicle is $20m/s$, and the road adhesion coefficient is 0.9.

In Figures 7 to 9, the dash-dot line represents the dynamic responses of the AGV with the LSC, that is, vehicle trajectory Y, β and γ, and the solid line represents the reference curves, that is, reference path $f_{road}(t)$, β^* and γ^*. In Figure 7, the AGV can effectively track the reference path. It completes automated driving under double lane change manoeuvre effectively. In Figures 8 and 9 the sideslip angle and yaw rate of the AGV using LSC can track the ideal reference curves accurately. Thus, the proposed control method can ensure the lateral stability of the AGVs in the process of lane change operation.

Case 2: Serpentine path manoeuvre

In this subsection, a serpentine path manoeuvre is carried out for AGVs, which evaluates the path tracking and the lateral stability performance of the AGV with the proposed scheme.

Scenario: the longitudinal speed of the vehicle is $30m/s$, and the road adhesion coefficient is 0.7.

In Figures 10 to 12, the dash-dot line represents the dynamic responses of the AGV with the LSC, that is, vehicle trajectory Y, β and γ, and the solid line represents the reference curves, that is, reference path $f_{road}(t)$, β^* and γ^*. In Figure 10, the AGV can effectively track the reference path. In Figures 11 and 12 the sideslip angle and yaw rate of the AGV with LSC can track the ideal reference curves accurately. Thus, the proposed control method can ensure the lateral stability of the AGVs.

The simulation results from Case 1 and Case 2 clearly indicate the effectiveness of the proposed method across various driving speeds and reference
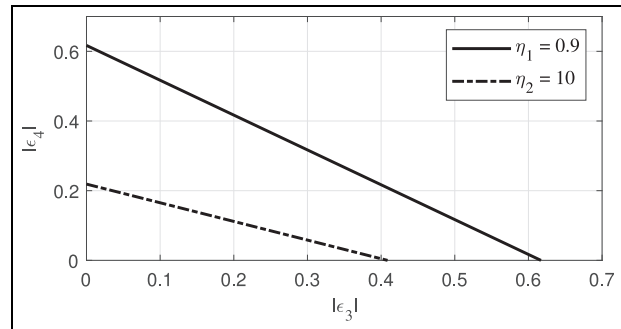
Figure 6. Controller parameter settings.

paths, providing strong evidence for the efficacy of the steering strategy. Moreover, the vehicle exhibits an ideal response in terms of sideslip angle and yaw rate, thereby showing the effectiveness of ESO-SMC in accurately tracking the reference signals.

Case 3: Double lane change manoeuvre with disturbances

Note that the ESO-SMC is designed to accurately track the reference signal in the presence of disturbances in this paper. In order to verify the effectiveness of the proposed controller under disturbances, a linear quadratic regulator (LQR) is carried out to track the reference signal under the same driving condition, in which the steering strategy and reference model are the same as the LSC. As shown in Figure 13, the scheme of control system is referred to as SR-LQR in this paper. The parameters of LQR are

$$Q = \begin{bmatrix} 40 & 0 \\ 0 & 15 \end{bmatrix}, R = \begin{bmatrix} 1 & 0 \\ 0 & 1 \end{bmatrix} \tag{35}$$

Scenario: the vehicle's longitudinal speed is $20m/s$, the wet cement pavement with a road adhesion coefficient is 0.6 and the crosswind with the speed of $5m/s$ is acted at the centroid of the vehicle body.

In Figures 14 to 16, the dash-dot line and the dash line represent the dynamic responses of AGV with the LSC and the SR-LQR, respectively, that is, Y, β and γ, and the solid line represents the reference curve, that is, reference path $f_{road}(t)$, β^* and γ^*.

In Figure 14, both of the AGVs with the LSC and the SR-LQR can effectively follow the reference path. It shows the proposed steering strategy can complete automated driving under double lane change manoeuvre effectively. Furthermore, the yaw rate's responses of AGV also show that the proposed steering strategy can ensure the performance of path tracking. In Figure 15, both of them can track the ideal yaw rate that influences the vehicle lateral displacement. In Figure 16, ESO-SMC can track the reference signal with a smaller error when vehicle is under cross-wind disturbances. The large sideslip angle of AGV with the
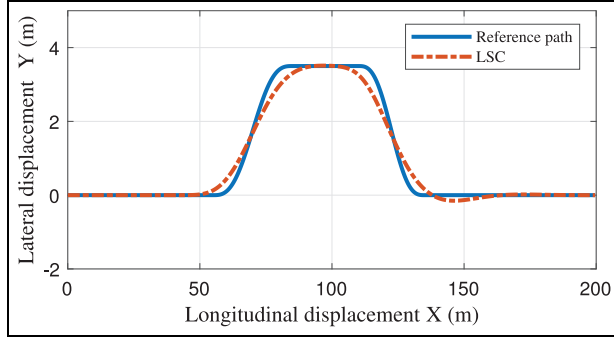
Figure 7. Path tracking performance in Case 1 (the blue line represents the reference path, and the red line represents the trajectory of AGVs with the LSC).
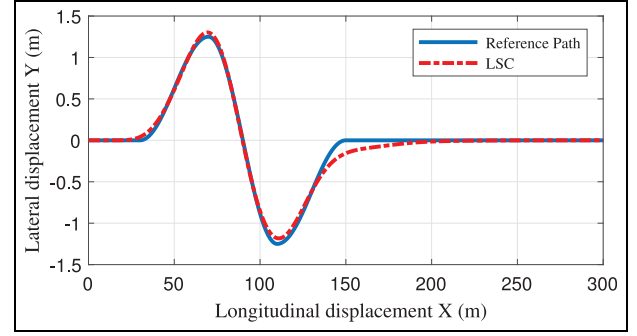

Figure 10. Path tracking performance in Case 2 (the blue line represents the reference path, and the red line represents the trajectory of AGV with the LSC).
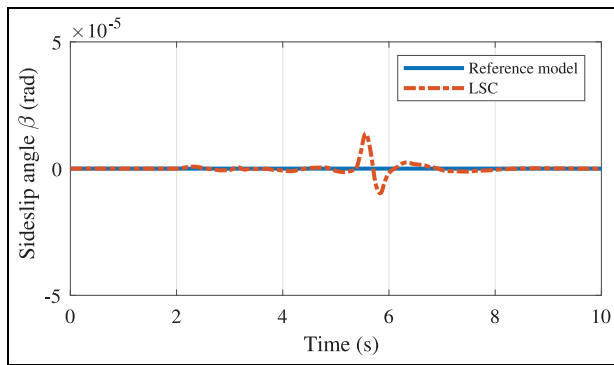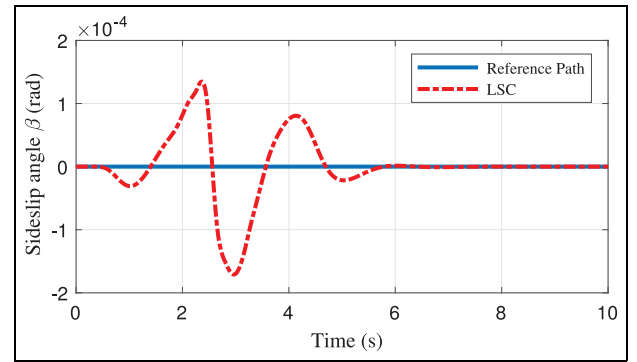

Figure 8. Slip angle response in Case 1.

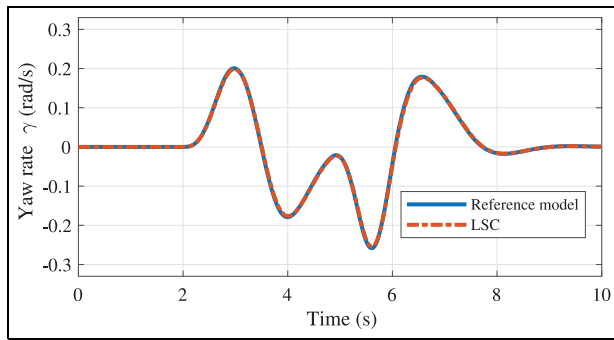**Figure 11.** Slip angle response in Case 2.
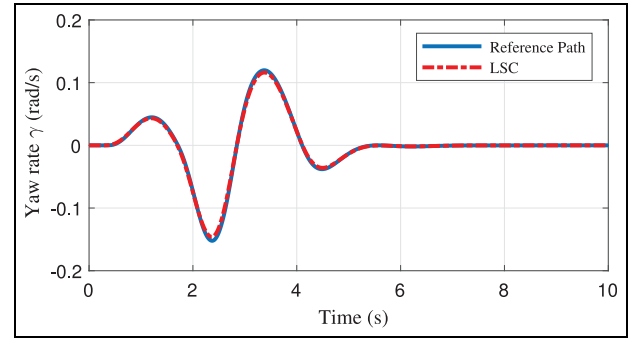

Figure 9. Yaw rate response in Case 1.

Figure 12. Yaw rate response in Case 2.

SR-LQR has a negative influence on the lateral stability at the same time. The proposed control method can complete autonomous driving, and ensure the vehicle lateral stability with respect to cross-wind disturbances.

Case 4: Double lane change manoeuvre under different sprung masses

In general, the cornering stiffness perturbations are caused by the time-varying tyre load variation, that is, time-varying sprung masses. The lane change manoeuvres under different sprung masses are carried out in this section.

Scenario: The vehicle longitudinal speed is $20 m/s$, the road adhesion coefficient is 0.9, the vehicle load is added to $1500 kg$ and the LQR parameters are the same as (35).

In Figures 17 to 19, the dash-dot line and the dash line represent the dynamic responses of AGV with the LSC and the SR-LQR, respectively, that is, vehicle trajectory Y, β γ, and the solid line represents the reference curve, that is, reference path $f_{road}(t)$, β^* γ^*. AGVs can follow the reference path with different stability controller, as shown in Figure 17. Furthermore, both the AGVs with the LSC and the SR-LQR can effectively track the idea yaw rate, c.f., Figures 17 and 18. In
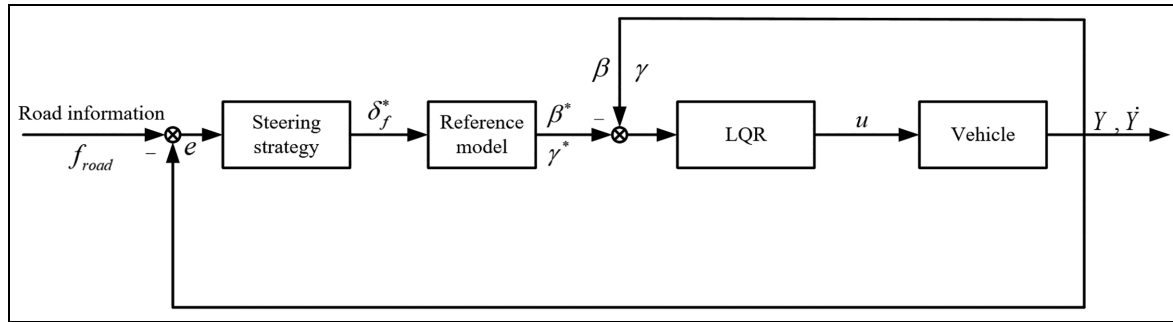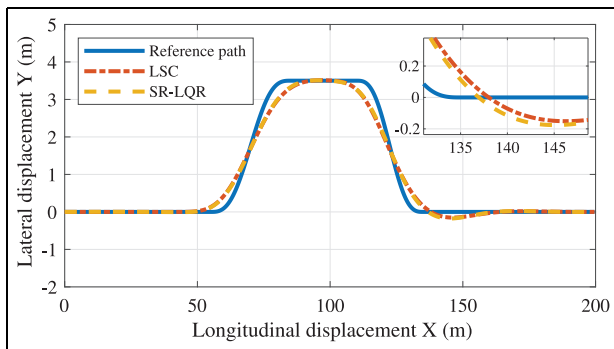
Figure 13. The control system of AGV with LQR.

Figure 14. Path tracking performances in Case 3 (the blue line represents the reference path, the red line represents the trajectory of AGV with the LSC and the orange line represents the trajectory of AGV with the SR-LQR).
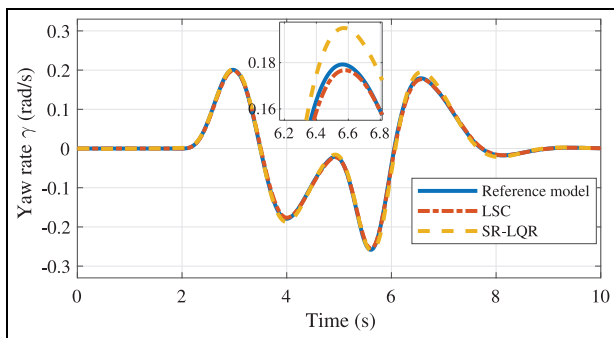

Figure 16. Yaw rate response in Case 3.

Figure 15. Slip angle response in Case 3.

Figure 17. Path tracking performances in Case 4 (the blue line represents the reference path, the red line represents the trajectory of AGV with the LSC and the orange line represents the trajectory of AGV with the SR-LQR).

Figure 19, the LSC can track the ideal references with a smaller error when the vehicle load is added to $1500\,kg$. In summary, the proposed control scheme can achieve automated driving and ensure vehicle lateral stability even in the presence of parameter perturbations.

Conclusion

A novel lateral stability controller combined with a steering strategy, reference model and an ESO-SMC was presented in this paper. The steering strategy was designed to obtain the ideal front wheel steering angle, in which a fuzzy algorithm was adopted to adjust real-
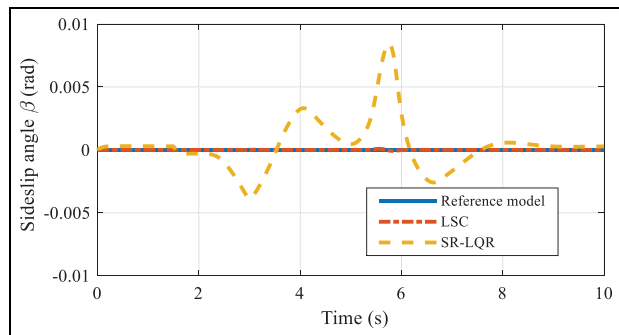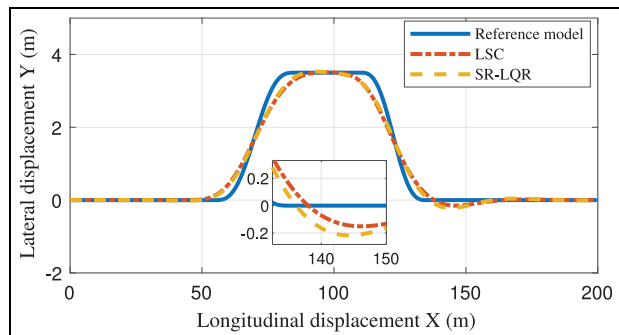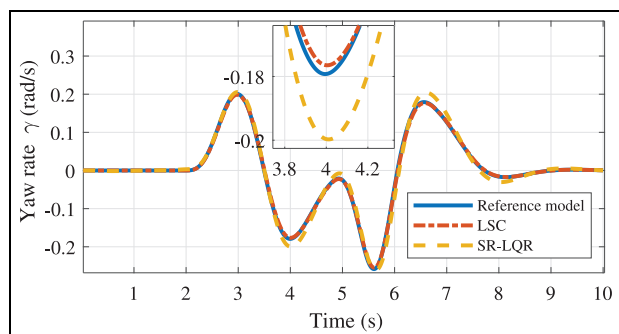

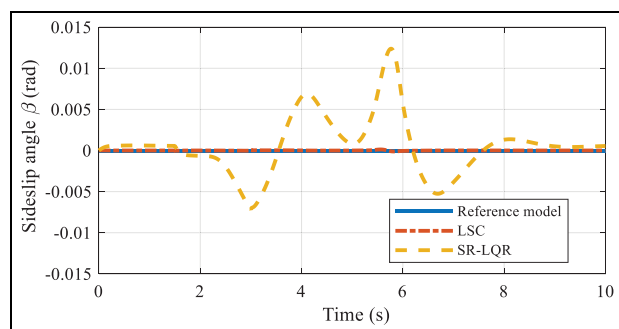**Figure 18.** Slip angle response in Case 4.

Figure 19. Yaw rate response in Case 4.

time the parameters of steering strategy. The ESO-SMC was designed to observe and compensate the disturbances and the unmeasured state. Simulation results show that the proposed scheme can accurately track the reference path and effectively improve the lateral stability, and dramatically reduce the influence of uncertainties.

The control problem under the constant vehicle longitudinal speed is addressed, whereas the control of the longitudinal speed is not taken into account in the present paper. Future research will take the time-varying longitudinal speed of vehicles into account.

Declaration of conflicting interests

The author(s) declared no potential conflicts of interest with respect to the research, authorship, and/or publication of this article.

Funding

ORCID iD

Shuyou Yu https://orcid.org/0000-0002-3258-6494

References

1. Amer NH, Hudha K, Zamzuri H, et al. Adaptive modified Stanley controller with fuzzy supervisory system for trajectory tracking of an autonomous armoured vehicle. *Robot Auton Syst* 2018; 105: 94–111.
2. Reina G, Milella A and Underwood J. Self-learning classification of radar features for scene understanding. *Robot Auton Syst* 2012; 60: 1377–1388.
3. Dickmann J, Klappstein J, Hahn M, et al. Automotive radar the key technology for autonomous driving: from detection and ranging to environmental understanding. In: *2016 IEEE radar conference (RadarConf)*, Philadelphia, PA, USA, 2–6 May 2016, pp.1–6. New York: IEEE.
4. Wang J, Zheng H and Zong C. Longitudinal and lateral dynamics control of automatic lane change system. *Trans Inst Meas Contr* 2019; 41: 4322–4338.
5. Chen C, Jia Y, Shu M, et al. Hierarchical adaptive path-tracking control for autonomous vehicles. *IEEE Trans Intell Transp Syst* 2015; 16: 2900–2912.
6. Al-Mayyahi A, Wang W and Birch P. Design of fractional-order controller for trajectory tracking control of a nonholonomic autonomous ground vehicle. *J Contr Autom Electr Syst* 2016; 27: 29–42.
7. Guo K and Guan H. Modelling of driver/vehicle directional control system. *Veh Syst Dyn* 1993; 22: 141–184.
8. Lee T, Kang J, Yi K, et al. An investigation on the integrated human driver model for closed-loop simulation of intelligent safety systems. *J Mech Sci Technol* 2010; 24: 761–767.
9. Ding H, Guo K, Wan F, et al. An analytical driver model for arbitrary path following at varying vehicle speed. *Int J Veh Auton Syst* 2007; 5: 204–218.
10. Xu S and Peng H. Design, analysis, and experiments of preview path tracking control for autonomous vehicles. *IEEE Trans Intell Transp Syst* 2020; 21: 48–58.
11. Wang Y, Bian N, Li J, et al. A triple-step non-linear control for path following of autonomous vehicles with uncertain kinematics and dynamics. *IET Control Theory Appl* 2017; 11: 3381–3387.
12. Hu C, Jing H, Wang R, et al. Robust H∞ output-feedback control for path following of autonomous ground vehicles. *Mech Syst Signal Process* 2016; 70: 414–427.
13. Hang P, Chen X and Luo F. LPV/H∞ controller design for path tracking of autonomous ground vehicles through four-wheel steering and direct yaw-moment control. *Int J Autom Technol* 2019; 20: 679–691.
14. Jin M, Lee J, Chang PH, et al. Practical nonsingular terminal sliding-mode control of robot manipulators for high-accuracy tracking control. *IEEE Trans Ind Electron* 2009; 56: 3593–3601.
15. Lv S, Wang N, Wang Y, et al. Nonsingular terminal sliding mode based trajectory tracking control of an autonomous surface vehicle with finite-time convergence. In: Cong F, Leung A and Wei Q (eds) *Advances in neural networks-ISNN 2017: 14th international symposium, ISNN 2017*. Cham: Springer, 2017, pp.83–92.
16. Wang X and Li S. Finite-time trajectory tracking control of under-actuated autonomous surface vessels based on non-singular terminal sliding mode. *Aust J Electr Electron Eng* 2012; 9: 235–246.
17. Wu Y, Wang L, Zhang J, et al. Path following control of autonomous ground vehicle based on nonsingular terminal sliding mode and active disturbance rejection control. *IEEE Trans Veh Technol* 2019; 68: 6379–6390.
18. Yoshida H, Shinohara S and Nagai M. Lane change steering manoeuvre using model predictive control theory. *Veh Syst Dyn* 2008; 46: 669–681.
19. Falcone P, Borrelli F, Asgari J, et al. Predictive active steering control for autonomous vehicle systems. *IEEE Trans Control Syst Technol* 2007; 15: 566–580.
20. Yu S, Guo Y, Meng L, et al. MPC for path following problems of wheeled mobile robots. *IFAC-PapersOnLine* 2018; 51: 247–252.

21. Liu Y, Yu S, Guo Y, et al. Receding horizon control for path following problems of wheeled mobile robots. *Control Theory Appl* 2017; 34: 424–432.

22. Kuutti S, Bowden R, Jin Y, et al. A survey of deep learning applications to autonomous vehicle control. *IEEE Trans Intell Transp Syst* 2021; 22: 712–733.

23. Moon S, Moon I and Yi K. Design, tuning, and evaluation of a full-range adaptive cruise control system with collision avoidance. *Control Eng Pract* 2009; 17: 442–455.

24. Chen J, Shuai Z, Zhang H, et al. Path following control of autonomous four-wheel-independent-drive electric vehicles via second-order sliding mode and nonlinear disturbance observer techniques. *IEEE Trans Ind Electron* 2021; 68: 2460–2469.

25. Shufeng W and Junyou Z. Performance analysis of 4WS vehicle based on different control strategy. In: *2009 Chinese control and decision conference*, Guilin, China, 17–19 June 2009, pp.5401–5404. New York: IEEE.

26. Tan L, Yu S, Guo Y, et al. Sliding-mode control of four wheel steering systems. In: *2017 IEEE international conference on mechatronics and automation (ICMA)*, Takamatsu, Japan, 6–9 August 2017, pp.1250–1255. New York: IEEE.

27. Shi K, Yuan X and He Q. Double-layer dynamic decoupling control system for the yaw stability of four wheel steering vehicle. *Int J Control Autom Syst* 2019; 17(5): 1255–1263.

28. Xu FX, Liu XH, Chen W, et al. Improving handling stability performance of four-wheel steering vehicle based on the H2/H∞ robust control. *Appl Sci* 2019; 9(5): 857.

29. Yu S, Li W, Wang W, et al. Nonlinear control of active four wheel steer-by-wire vehicles. *IEEE Access* 2019; 7: 127117–127127.

30. Priyanka EB, Maheswari C and Thangavel S. Online monitoring and control of flow rate in oil pipelines transportation system by using PLC based fuzzy-PID controller. *Flow Meas Instrum* 2018; 62: 144–151.

31. Jin X, Chen K, Zhao Y, et al. Simulation of hydraulic transplanting robot control system based on fuzzy PID controller. *Measurement* 2020; 164: 108023.

32. Nagai M, Shino M and Gao F. Study on integrated control of active front steer angle and direct yaw moment. *JSAE Rev* 2002; 23: 309–315.

33. Yang X, Wang Z and Peng W. Coordinated control of AFS and DYC for vehicle handling and stability based on optimal guaranteed cost theory. *Veh Syst Dyn* 2009; 47: 57–79.

34. Liu C, Sun W and Zhang J. Adaptive sliding mode control for 4-wheel SBW system with Ackerman geometry. *ISA Trans* 2020; 96: 103–115.

35. Zheng H, Yang S and Li B. Optimization control for 4WIS electric vehicle based on the coincidence degree of wheel steering centers. *SAE Int J Veh Dyn Stab NVH* 2018; 2(3): 169–184.

36. Russell HEB and Gerdes JC. Design of variable vehicle handling characteristics using four-wheel steer-by-wire. *IEEE Trans Control Syst Technol* 2016; 24: 1529–1540.

37. Sira-Ramirez H and Oliver-Salazar MA. On the robust control of buck-converter DC-motor combinations. *IEEE Trans Power Electron* 2013; 28: 3912–3922.

38. Chen JIE, Patton RJ and Zhang HY. Design of unknown input observers and robust fault detection filters. *Int J Control* 1996; 63: 85–105.

39. Chen MS, Hwang YR and Tomizuka M. A state-dependent boundary layer design for sliding mode control. *IEEE Trans Automat Contr* 2002; 47: 1677–1681.

40. Yu S, Feng Y and Yang X. Extended state observer–based fractional order sliding-mode control of piezoelectric actuators. *Proc IMechE, Part I: J Systems and Control Engineering* 2021; 235: 39–51.

41. Esmailzadeh E, Vossoughi GR and Goodarzi A. Dynamic modeling and analysis of a four motorized wheels electric vehicle. *Veh Syst Dyn* 2001; 35: 163–194.